Journal of Power Sources 196 (2011) 379–385

Contents lists available at ScienceDirect

Journal of Power Sources

journal homepage: www.elsevier.com/locate/jpowsour

Enhanced rate capability of multi-layered ordered porous nickel phosphide film as anode for lithium ion batteries

J.Y. Xiang, X.L. Wang*, J. Zhong, D. Zhang, J.P. Tu*

State Key Laboratory of Silicon Materials, Department of Materials Science and Engineering, Zhejiang University, Hangzhou 310027, China

ARTICLE INFO

Article history:
Received 16 April 2010
Received in revised form 11 June 2010
Accepted 21 June 2010
Available online 25 June 2010

Keywords:
Nickel phosphide
Porous film
Electrodeposition
Anode
Lithium ion battery

ABSTRACT

Porous nickel phosphide films are fabricated by electrodeposition through self-assembled polystyrene sphere multi-layers as template. After the removal of the template, well-ordered and close-packed spherical pores are left in the films. The thin walls of the adjacent pores make up a three-dimensional network nanostructure in the triple-layer porous Ni_3P film. The as-prepared triple-layer porous film delivers significantly enhanced rate capability over the single- and double-layer ones. After 50 cycles, the capacity of the triple-layer Ni_3P porous film still sustains 557 mAh g^{-1} and 243 mAh g^{-1} at a charge–discharge rate of 0.2 C and 5 C (1 C = 388 mA g^{-1}), respectively. According to the analysis of electrochemical impedance spectrum (EIS), the improved electrochemical performance of the triple-layer film can be attributed to the fast migration of Li^+ through surface-passivating layer and the facilitated charge transfer into Ni_3P three-dimensional network nanostructure.

1. Introduction

In the last decade, many efforts were devoted to seeking for new materials as anodes for next-generation lithium ion batteries (LIBs), which can show higher capacity than graphite while exhibit excellent cyclability at the same time. One of the promising anode materials is the transition metal phosphide (M–P, where M = Fe, Co, Ni, Cu, etc.) for its high gravimetric and volumetric capacity associated with the low electrode volume expansion [1–4]. The electrochemical conversion mechanism of M–P toward Li^+ is commonly considered as [5–7]:

$$MP_y + 3yLi^+ + 3ye^- \Leftrightarrow yLi_3P + M^0 \quad (1)$$

However, the capacity retention of these phosphides is somewhat disappointing for the limited electrode reaction kinetics [2,8–10]. Construction of nanoarchitectures is an effective approach to enhance the cyclability of the transition metal phosphides for the sufficient contact of active material/electrolyte and the short diffusion length of Li^+ in the nanostructures. Therefore, hollow Cu_3P spheres [11,12], FeP nanocrystals [13], hollow Ni_2P nanoparticles [14] have been synthesized in recent years.

Even though, in the normal LIBs, electrode is commonly prepared by mixing active material with polymer binder, which probably negates the favorable effects of the decreasing particle size and introduces supplementary undesirable interfaces [15]. An alternative way to obviate this problem is fabricating nanoarchitectured film directly on current collector. Thus, the advantages of nanostructured material can be fully utilized. Among the various approaches for preparing nanostructured films, electrodeposition is considered as a competitive method for its facility and well-controlling. Lately, porous Sn-based alloy films [16,17] and hierarchical porous Co_3O_4 films [18] have been prepared by electrodeposition through colloidal crystal as template. However, to our knowledge, there is few work on the synthesis of porous transition metal phosphide film and its application as anode for LIBs. Therefore, in the present work, we firstly report the fabrication of multi-layered ordered porous nickel phosphide film by electrodeposition through self-assembled monodisperse polystyrene sphere template. The effect of layer number on electrochemical performances of porous Ni_3P electrodes is intensely studied.

2. Experimental

2.1. Assembly of monodisperse polystyrene sphere multi-layers

Firstly, one layer of monodisperse polystyrene spheres was assembled on a chemical polished copper foil (99.9%). The diameter of the sphere used in this work was about 500 nm. The detailed procedures were according to Ref. [18]. After the monolayer was dried at room temperature, a second and third polystyrene sphere layer was subsequently assembled on the as-prepared monolayer by repeating the same procedures. At last, three layers of monodisperse polystyrene

* Corresponding author. Tel.: +86 571 87952573; fax: +86 571 87952856.
E-mail addresses: wangxl@zju.edu.cn (X.L. Wang), tujp@zju.edu.cn (J.P. Tu).

0378-7753/$ – see front matter © 2010 Elsevier B.V. All rights reserved.
doi:10.1016/j.jpowsour.2010.06.068

spheres were successfully fabricated on the copper substrate.

2.2. Preparation and characterization of porous Ni_3P films

Porous Ni_3P films were electrodeposited in a three-electrode system with the as-prepared polystyrene sphere templates on copper substrate as the working electrode, a Pt foil as the counter electrode and a saturated calomel electrode (SCE) as the reference electrode. The compositions of the electrolyte were 0.6 M $NiSO_4{\cdot}6H_2O$, 0.2 M $NiCl_2{\cdot}6H_2O$, 0.8 M H_3BO_3 and 0.6 M $NaH_2PO_4{\cdot}H_2O$. The electrodepositing process was carried out at a current density of 0.02 A cm^{-2} at 55 °C for different times. Afterwards, the samples were immersed into toluene for 24 h to remove the polystyrene sphere templates. Finally, the as-prepared films were heated at 500 °C for 1 h under the flowing argon atmosphere and cooled with furnace to room temperature.

The structure and surface morphology of the porous Ni_3P films were characterized by X-ray diffraction (XRD, Rigaku D/max with Cu Kα radiation) and field emission scanning electron microscopy (FESEM, FEI SIRON and Hitachi S-4700), respectively.

2.3. Electrochemical measurements

Electrochemical performances of the porous Ni_3P films were investigated in a coin-type cell (CR 2025), which was assembled following the procedures in Ref. [19]. The galvanostatic charge–discharge tests were conducted on LAND battery test system at different rates from 0.02 V to 3.0 V (versus Li/Li^+) at room temperature (25 ± 1 °C). Cyclic voltammetry (CV) and electrochemical impedance spectrum (EIS) were performed on CHI660C electrochemical workstation. EIS tests were performed using a three-electrode cell with the prepared Ni_3P films as the working electrode, metallic lithium foil as both the counter and reference electrodes.

3. Results and discussion

Fig. 1 shows the morphology of the Ni_3P film electrodeposited through one layer of monodisperse polystyrene spheres for 5 min. After the removal of the template, the spherical pores left in the film are close-packed and well-ordered (Fig. 1a). The diameter of the spherical pore is about 500 nm, as same as that of the polystyrene sphere (Fig. 1b). On the side view (Fig. 1c), it is seen that the spherical pores arranging in the film actually look like open bowls and the walls of these "bowls" are only about 50–80 nm in thickness. When the two layers of monodisperse polystyrene spheres are used as the template, porous Ni_3P film can also be obtained by electrodepositing for 10 min as shown in Fig. 2a and b. On the side view in Fig. 2c, two layers of spherical pores are arranged orderly in the film. The diameter of these pores is also about 500 nm and the thickness of the film is about 1 μm.

The SEM images of the Ni_3P film electrodeposited through the three layers of polystyrene spheres for 15 min are given in Fig. 3. The well-ordered and close-packed "open bowls" also appear in the film (Fig. 3a and b). On the side view in Fig. 3c, it is discovered that the film consists of three layers of spherical pores, and the thin walls connecting the adjacent pores make up a three-dimensional network nanostructure. What is interesting is that the upper porous layer shifts from the lower layer by a distance exactly equal to the pore diameter (Fig. 2c and 3c). It is believed that the stacking manner of the pores is mainly decided by the assembling manner of the polystyrene sphere multi-layers (see the model in Fig. 3d). Bartlett et al. [20] consider this stacking is similar to the packing sequence of face-centered cubic (fcc) structure (ABCABC. . .sequence) with (1 1 1) plane paralleling to the substrate. The total thickness of the three-dimensional porous Ni_3P film is about 1.5 μm.

In the present work, we define the as-deposited Ni_3P films in Figs. 1–3 as single-, double- and triple-layer films, respectively. The loading weights of the three films on copper foils are 0.65 mg cm^{-2}, 1.43 mg cm^{-2} and 2.21 mg cm^{-2}, respectively, which are calculated by comparing the weights of the copper substrates before and after electrodeposition. Moreover, the apparent surface area (contact area between Ni_3P and electrolyte) can also be approximatively calculated since the size and arrangement of the pores in the three films are almost the same. We suppose that each pore is 500 nm in diameter and the wall is 50 nm in thickness. The electrode plate is 12 mm in diameter. So, it is calculated that the apparent surface area per unit mass of the three films are 2.01×10^3 cm^2 g^{-1}, 2.72×10^3 cm^2 g^{-1} and 2.93×10^3 cm^2 g^{-1}; the apparent surface

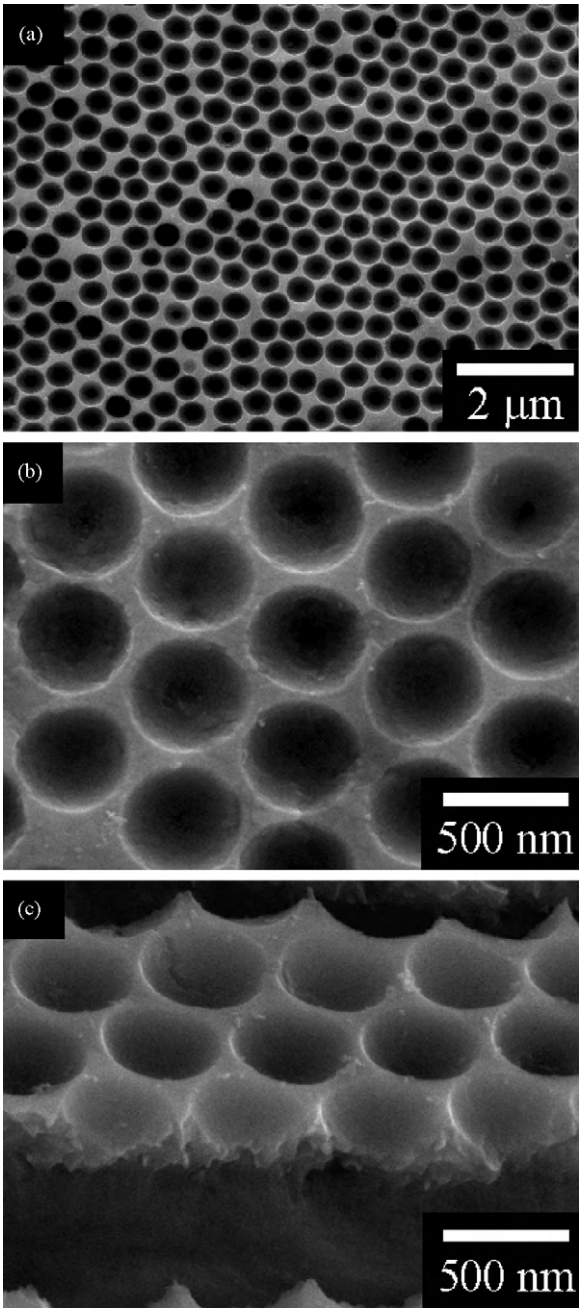

Fig. 1. SEM images of the porous Ni_3P film electrodeposited through one layer of polystyrene spheres for 5 min.

area per unit electrode area are 1.30, 3.89, and 6.49, respectively. As can be seen, the value of apparent surface area per unit mass of the three films is closed to each other, while the apparent surface area per unit electrode area is quite different. The triple-layer Ni_3P film exhibits the largest contact area with electrolyte per unit electrode area.

Fig. 4 presents the XRD pattern of the single-layer film after treated at 500 °C for 1 h. Ni_3P is the main phase in the film with a tetragonal structure (I4 space group, JCPDS 34-0501). Besides, metallic Ni with a cubic structure (Fm3m space group, JCPDS 04-0850) is also detected as a side product. Although the as-deposited Ni_3P film is not a pure one, the side product nickel will play a positive role (facilitate the decomposition of Li_3P and make the charge reaction $3Ni + Li_3P \Leftrightarrow Ni_3P + 3Li^+ + 3e^-$ proceed to a higher extent) when the film is used as anode for LIBs. It has been discussed intensively in our previous work [7]. The XRD patterns of the double- and triple-layer porous films are similar to the pattern in Fig. 4.

The cyclability of these porous Ni_3P films at different discharge–charge rates is shown in Fig. 5a. The first capacities of the single-, double- and triple-layer Ni_3P films are 700 mAh g^{-1}, 739 mAh g^{-1}, and 794 mAh g^{-1} at a rate of 0.2 C (1 C = 388 mA g^{-1}),

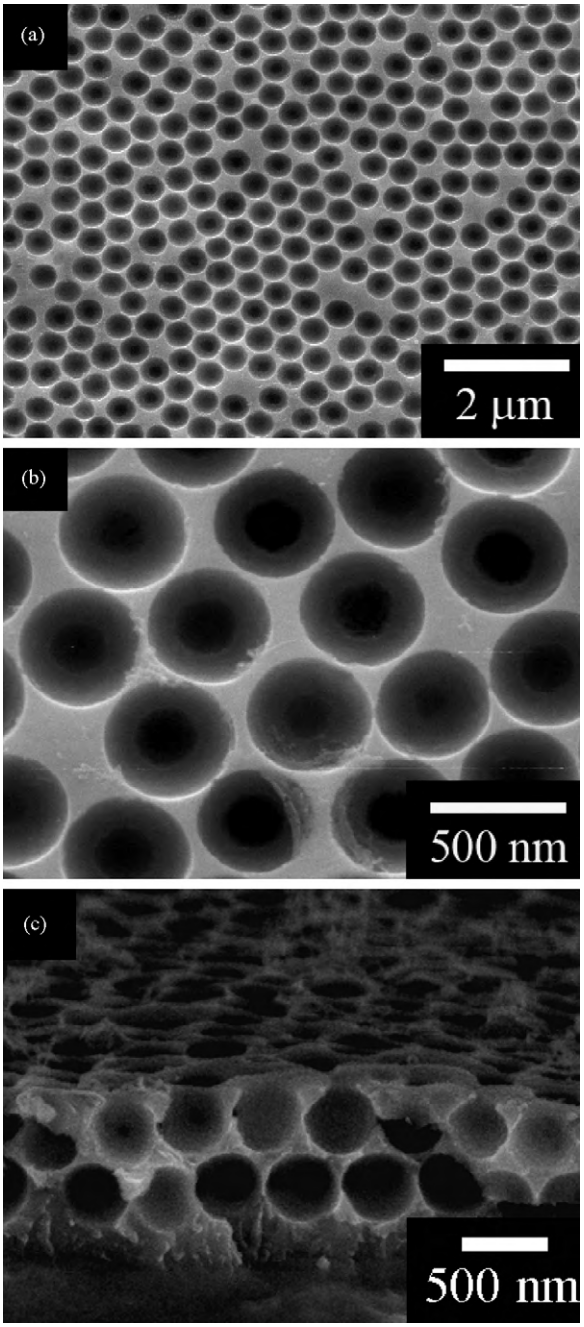

Fig. 2. SEM images of the porous Ni_3P film electrodeposited through two layers of polystyrene spheres for 10 min.

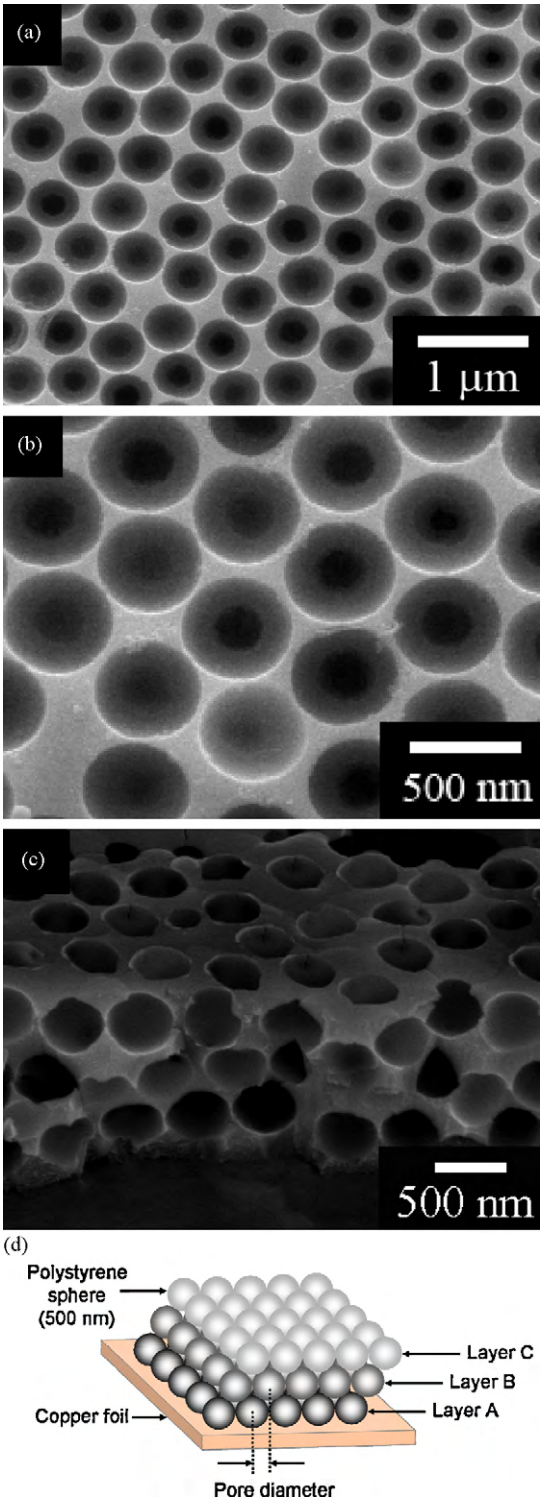

Fig. 3. (a)–(c) SEM images of the porous Ni_3P film electrodeposited through three layers of polystyrene spheres for 15 min and (d) schematic illustration for the stacking manner of pores in the film.

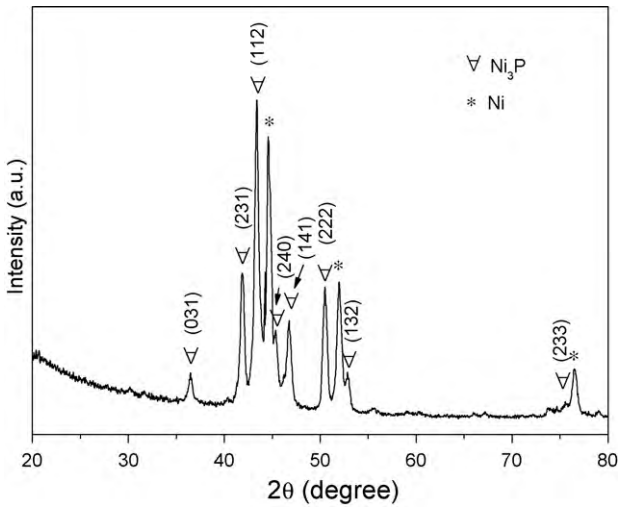

Fig. 4. XRD pattern of the porous Ni_3P film electrodeposited through one layer of polystyrene spheres.

respectively. The high initial capacities indicate large areas of solid electrolyte interfaces (SEI) are formed in the porous structures during the initial discharge process. After 50 cycles, all the three porous Ni_3P electrodes exhibit high reversible capacities which are higher than 500 mAh g^{-1}, as shown in Fig. 5b. It is ascribed to the porous nanostructure which provides sufficient contact area of active material/electrolyte and shortens the diffusion length of Li^+ (50–80 nm). However, as the rate increases, the three porous Ni_3P electrodes show different capacity retentions. The capacity fading of the triple-layer film is much slower than that of the other two ones, especially at high rate. In Fig. 5b, it is seen that the reversible capacity of the triple-layer porous film still maintains 243 mAh g^{-1} at a discharge–charge rate of 5 C. The reversible capacity sustains 44% as the discharge–charge rate even rises 25 times. For the single- and double-layer films, the reversible capacities are only 124 mAh g^{-1} and 190 mAh g^{-1} at 5 C, respectively. In addition, the dependence of coulombic efficiency on cycle number of the porous Ni_3P electrodes at a discharge–charge rate of 1 C is provided in Fig. 5c. In the first five cycles, the triple-layer porous film exhibits significantly enhanced coulombic efficiency comparing with the other two ones. And in the subsequent cycles, the coulombic efficiency of the triple-layer porous film stays near 99%, which is still higher and more stable than that of the other two porous films (inset of Fig. 5c). The different rate capability and reversibility of the three porous electrodes indicate the different electrode reaction kinetics in the single-, double- and triple-layer films. The mechanism will be discussed later in the text.

Fig. 6 a–c show the cyclic voltammetry curves for the porous Ni_3P films from the 2nd to 4th cycle at scanning rates of 0.1 mV s^{-1}, 0.5 mV s^{-1} and 1.0 mV s^{-1}, respectively. The electrochemical behaviors of these electrodes are similar to each other. The cathodic and anodic peaks in the curves are indexed to the discharge reaction $Ni_3P + 3Li^+ + 3e^- \Leftrightarrow Li_3P + 3Ni$ and the corresponding charge reaction, respectively. As the scanning rate rises, the cathodic peak shifts to a lower potential and the anodic peak shifts to a higher potential. Besides, the peak current also increases accordingly, which is related to the Li^+ diffusion within the active material [21]. Among the three electrodes, the triple-layer Ni_3P film shows the smallest separation between the cathodic and anodic peaks, especially as the scanning rate rises. The comparison is clearly presented in Fig. 6d. As is known to all, the separation between the cathodic and anodic peaks has a close relationship with the polarization of the electrode. Smaller separation indicates lower polarization. Therefore, the polarization of the triple-layer porous Ni_3P film is the smallest, which means the charge-transfer delay on Ni_3P/electrolyte interfaces of the triple-layer film is not dramatic with the increasing rate. It is greatly attributed to the largest active surface area taken as the contact area between electrode and electrolyte of the triple-layer film. When a same current is applied, the actual exchange current density on the active interfaces of the triple-layer porous film is lower than those of the other two films. The exchange current density determines the actual rate of the electrode reaction [22]. Therefore, at a same discharge–charge rate, the exchange of lithium ions on Ni_3P/electrolyte interfaces of the triple-layer film is more sufficient than those of the single- and

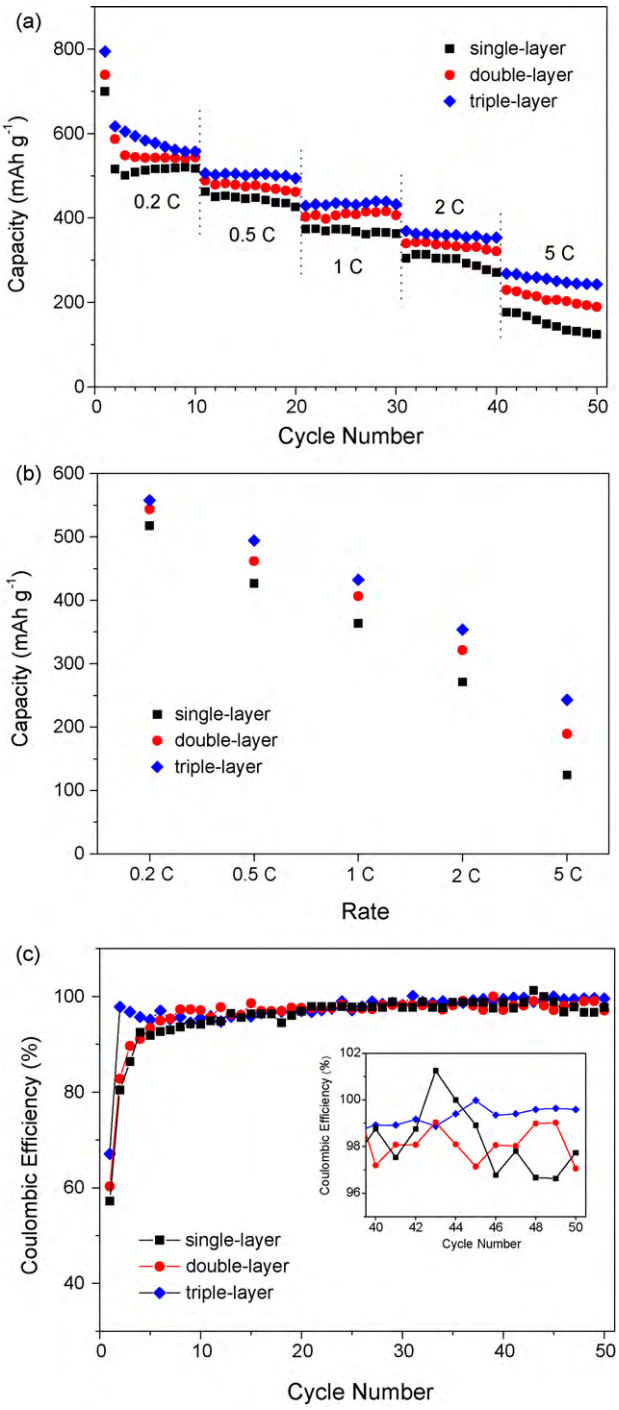

Fig. 5. (a) Cycling performances; (b) reversible capacities of the porous Ni_3P films at different rates and (c) coulombic efficiencies of the porous Ni_3P films at rate of 1 C.

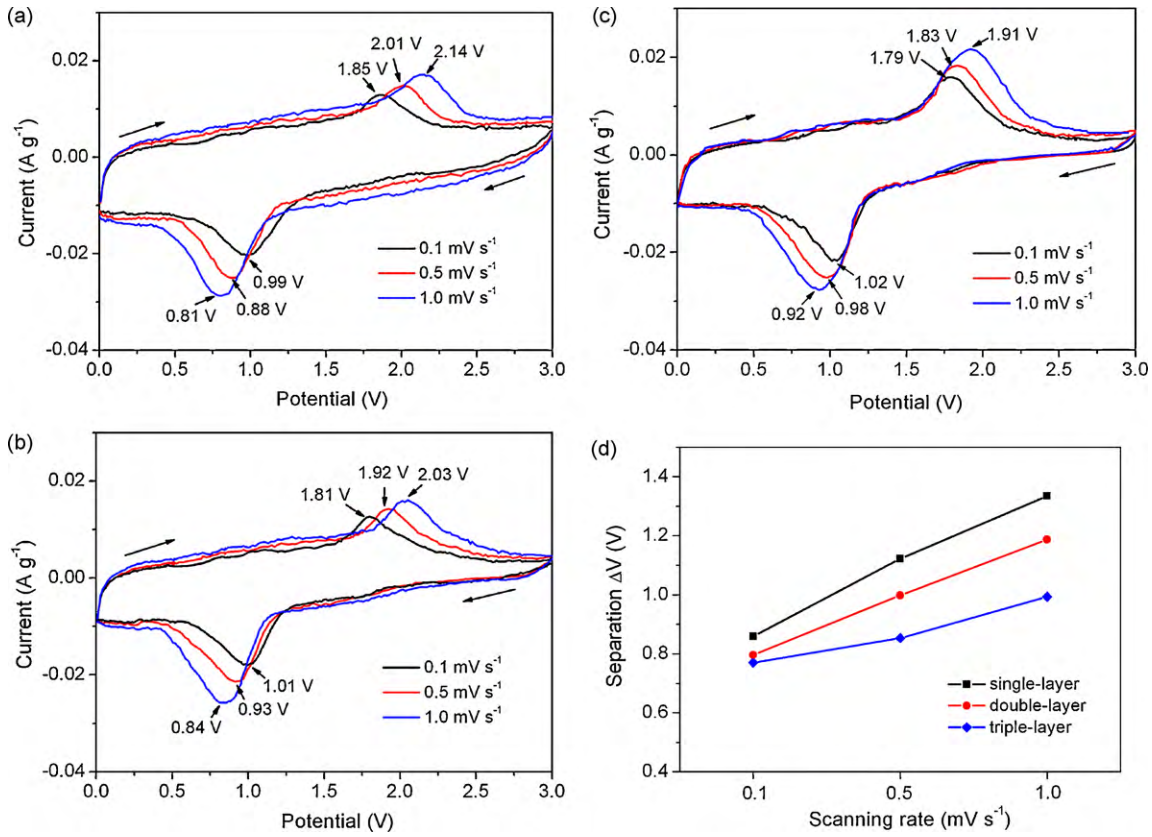

Fig. 6. Cyclic voltammetry curves for the (a) single-layer, (b) double-layer and (c) triple-layer Ni_3P films at different scanning rates from 0 V to 3.0 V; (d) The separation between the cathodic and anodic peaks of the Ni_3P electrodes at different scanning rates.

double-layer ones, which results in the decreasing polarization of the triple-layer porous electrode.

Electrochemical impedance spectrum (EIS) is used to understand the electrode reaction kinetics of these porous Ni_3P electrodes. The measurement was conducted in the frequency range from 0.01 Hz to 100 kHz after discharging the electrodes to 0.02 V (versus Li/Li^+) at 0.2 C in the 10th cycle. Theoretically speaking, regardless of the number of layers, the active surface condition of these porous films should be similar with each other since the films are prepared by the same polystyrene sphere template. However, the high-mediate frequency semicircle in the Nyquist plots, which indexed to the impedance of Li^+ migration through surface surface-passivating layer and further transfer into active material [23], is quite different among the three electrodes as presented in Fig. 7a and b. The triple-layer film exhibits the smaller high-mediate frequency semicircle than the single- and double-layer ones.

In order to clearly illustrate the different impedance responses of these porous electrodes, schematic models of a dense electrode with a flat surface and a porous electrode are provided in Fig. 7c and d, respectively. R_e indicates the electrolyte resistance; Z_s, Z_c and Z_w stand for the surface-passivating layer impedance, charge-transfer impedance and semi-infinite Li^+ diffusion impedance, respectively. At one certain site on active material/electrolyte interface, the electrical transport along each phase and the exchange of charge through solid/liquid interface are similar in the dense and porous electrodes. However, in a large scale, the electrical transportation and charge-transfer processes will be different. In porous structure, due to the large specific surface area, the electrical current can spread in various directions and the lithium ions can transfer at more sites on solid/liquid interfaces (Fig. 7d). Therefore, it can be simplified that the equivalent circuit model of a porous electrode is composed of several parallel-connected circuits of the dense electrodes.

According to this assumption, an equivalent circuit for the porous Ni_3P electrode is given in Fig. 7e. It is a two-parallel diffusion paths model accounting for Li^+ migration through surface-passivating layer and further transfer into active material. Similar analogue is also used to explain the impedance of porous composite electrodes [24]. R_{el} indicates the solution resistance; $R_{sl(i)}$ and $C_{sl(i)}$ stand for the migration of lithium ions and capacity of the surface-passivating layer, respectively; $R_{ct(i)}$ and $C_{dl(i)}$ designate the related charge-transfer resistance and double-layer capacitance, respectively; $Z_{W(i)}$ represents the diffusion-controlled Warburg impedance ($i = 1, 2$). Fig. 7f presents the excellent fitness between the simulated curves and the experimental Nyquist plots, which indicates the accuracy of the simulated model.

Based on the parallel diffusion paths model, it is considered that the model of the triple-layer electrode should contain more parallel branches than those of the single- and double-layer electrodes, since the triple-layer porous Ni_3P film exhibits the largest apparent surface area per unit electrode area than the other two ones. More parallel branches in the circuit will no doubt result in lower equivalent impedance. Therefore, the triple-layer porous film shows a lower impedance of Li^+ migration through surface-passivating layer and further transfer into active material, which reflects the decreasing diameter of high-mediate frequency semicircle in the Nyquist plots in Fig. 7a and b.

Additionally, the Warburg diffusion in the very low frequency is also investigated. The Warburg impedance Z_w can be expressed as the following formula [25]:

$$Z_w = \sigma(1-j)\frac{1}{\sqrt{\omega}} \quad (2)$$

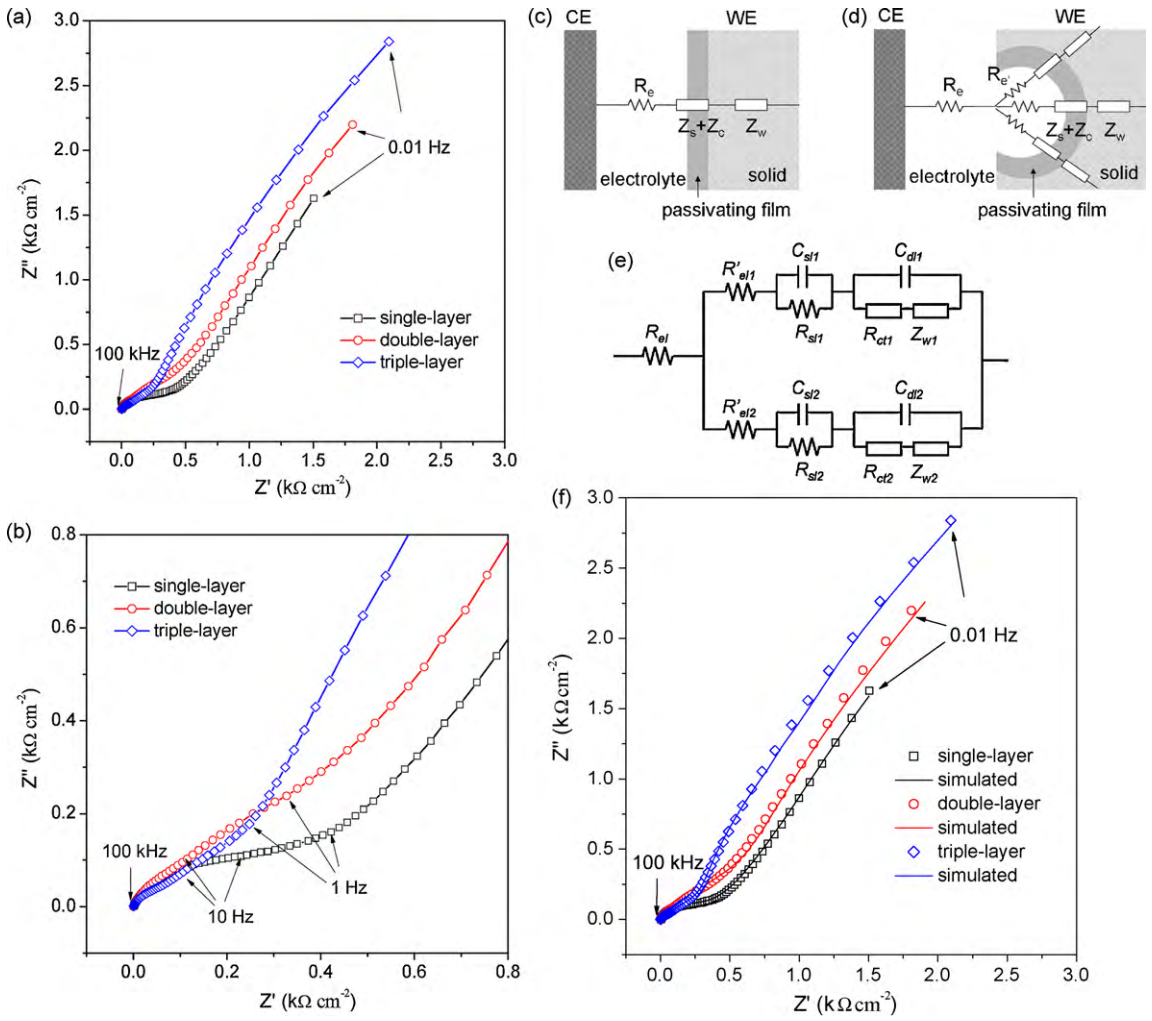

Fig. 7. (a) and (b) Nyquist plots of the porous Ni_3P electrodes in the frequency range from 0.01 Hz to 100 kHz after discharging the electrodes to 0.02 V in the 10th cycle; scheme of (c) a compact electrode with a flat surface and (d) a porous electrode; (e) equivalent circuit model for porous Ni_3P film electrode.

where σ is the Warburg coefficient and ω is the angular frequency. The σ can be obtained from the real resistance (Z') versus the inverse square root of the angular frequency ($\omega^{-1/2}$). The slopes of the straight lines in Fig. 8 are indexed to the Warburg coefficient of the three porous Ni_3P electrodes. It is obvious that the single-layer film shows the smallest Warburg coefficient while the triple-layer film exhibits the largest one. It is known to all that the larger value of σ indicates the smaller value of diffusion coefficient of Li^+ (D_{Li}). Thus, the impedance of lithium-ion diffusion within the triple-layer porous film is a little higher than that in the other two films. Even though, the effect of Warburg diffusion on the electrochemical performances could not be significant for the very short diffusion length of Li^+ in the as-prepared porous films (50–80 nm). Therefore, in this work, it is considered that the kinetics of Li^+ migration and charge transfer on active material/electrolyte interfaces is the key point to influence the electrochemical performances of the as-prepared porous Ni_3P films. The fast Li^+ migration through surface-passivating layer and the facilitated charge transfer on solid/liquid interfaces lead to the decreasing polarization and significantly enhanced capacity retention of the triple-layer film electrode.

It is worth mentioning that the nanoarchitectured film electrode cannot be blindly applied to such materials with thickness of several micrometers due to the significant decreasing kinetics during the electrochemical process with the increasing distance away from the current collector [15,26]. In this work, the thickness of the as-prepared triple-layer film is less than 2 μm, thus the decreasing electrical contact between active material and current

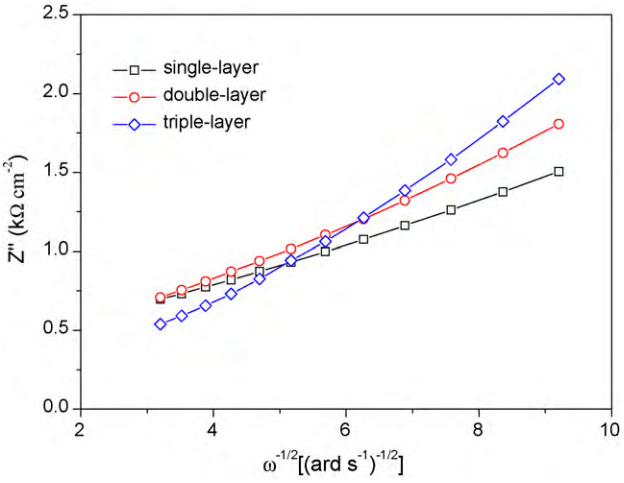

Fig. 8. The plots of the real resistance as a function of the inverse square root of angular frequency for the fully discharged porous Ni_3P electrodes in the frequency range from 0.01–0.1 Hz. (Data obtained from Fig. 7a).

collector with the increasing film thickness is so little that can be ignored.

4. Conclusions

Different porous Ni_3P films are prepared by electrodeposition through self-assembled polystyrene sphere multi-layers. The triple-layer film with a three-dimensional network nanostructure shows a significant improvement of electrochemical performances, especially the rate capability. The reversible capacity of the triple-layer Ni_3P film is 557 mAh g^{-1} and 243 mAh g^{-1} after 50 cycles at a charge–discharge rate of 0.2 C and 5 C, respectively. The reversible capacity still sustains 44% as the discharge–charge rate rises even 25 times. It is much higher than those of the single- and double-layer ones. The enhanced rate capability of the triple-layer porous film is ascribed to the decreasing impedance of Li^+ migration through surface-passivating layer and further transfer into Ni_3P three-dimensional network nanostructure. The carbon-free, three-dimensional porous Ni_3P film offers new opportunity for producing the next-generation LIBs.

References

[1] V. Pralong, D.C.S. Souza, K.T. Leung, L. Nazar, Electrochem. Commun. 4 (2002) 516–520.
[2] M. Cruz, J. Morales, L. Sanchez, J. Santos-Pena, F. Martin, J. Power Sources 171 (2007) 870–878.
[3] S. Boyanov, J. Bernardi, F. Gillot, L. Dupont, M. Womes, J.M. Tarascon, L. Monconduit, M.L. Doublet, Chem. Mater. 18 (2006) 3531–3538.
[4] K. Wang, J. Yang, J. Xie, B. Wang, Z. Wen, Electrochem. Commun. 5 (2003) 480–483.
[5] C. Villevielle, F. Robert, P.L. Taberna, L. Bazin, P. Simon, L. Monconduit, J. Mater. Chem. 18 (2008) 5956–5960.
[6] O. Crosnier, L.F. Nazar, Electrochem, Solid State Lett. 7 (2004) A187–A189.
[7] J.Y. Xiang, J.P. Tu, X.L. Wang, X.H. Huang, Y.F. Yuan, X.H. Xia, Z.Y. Zeng, J. Power Sources 185 (2008) 519–525.
[8] Z.S. Zhang, J. Yang, Y.N. Nuli, B.F. Wang, J.Q. Xu, Solid State Ionics 176 (2005) 693–967.
[9] H. Pfeiffer, F. Tancret, T. Brousse, Electrochim. Acta 50 (2005) 4763–4770.
[10] M.P. Bichat, T. Politova, H. Pfeiffer, F. Tancret, L. Monconduit, J.L. Pascal, T. Brousse, F. Favier, J. Power Source 136 (2004) 80–87.
[11] X.J. Wang, K. Han, Y.J. Gao, F.Q. Wan, K. Jiang, J. Cryst. Growth 307 (2007) 126–130.
[12] S.L. Liu, Y.T. Qian, L.Q. Xu, Solid State Commun. 149 (2009) 438–440.
[13] A.E. Henkes, R.E. Schaak, Chem. Mater. 19 (2007) 4234–4242.
[14] R.K. Chiang, R.T. Chiang, Inorg. Chem. 46 (2007) 369–371.
[15] Y. Xie, C.Z. Wu, Dalton Trans. (2007) 5235–5240.
[16] F.S. Ke, L. Huang, H.H. Jiang, H.B. Wei, F.Z. Yang, S.G. Sun, Electrochem. Commun. 9 (2007) 228–232.
[17] F.S. Ke, L. Huang, J.S. Cai, S.G. Sun, Electrochim. Acta 52 (2007) 6741–6747.
[18] X.H. Xia, J.P. Tu, J.Y. Xiang, X.H. Huang, X.L. Wang, X.B. Zhao, J. Power Sources 195 (2010) 2014–2022.
[19] X.H. Huang, J.P. Tu, X.H. Xia, X.L. Wang, J.Y. Xiang, L. Zhang, Y. Zhou, J. Power Sources 188 (2009) 588–591.
[20] P.N. Bartlett, J.J. Baumberg, P.R. Birkin, M.A. Ghanem, M.C. Netti, Chem. Mater. 14 (2002) 2199–2208.
[21] J.R. Dahn, J.W. Jiang, L.M. Moshurchak, J. Electrochem. Soc. 152 (2005) A1283–A1289.
[22] J.P. Meyers, M. Doyle, R.M. Darling, J. Newman, J. Electrochem. Soc. 147 (2000) 2930–2940.
[23] M.D. Levi, D. Aurbach, J. Phys. Chem. B 101 (1997) 4630–4640.
[24] M.D. Levi, D. Aurbach, J. Phys. Chem. B 108 (2004) 11693–11703.
[25] D. Kaoru, M. Mohamed, U. Minoru, U. Isamu, J. Electrochem. Soc. 150 (2003) A425–A429.
[26] K. Nishikawa, K. Dokko, K. Kinoshita, S.-W. Woo, K. Kanamura, J. Power Sources 189 (2009) 726–729.